Diluted orbital degeneracy and large orthorhombic distortions in ferrimagnetic spinel $Cu_xMn_{3-x}O_4$

Kee Hwan Lee, Hun Chang, In Yong Hwang, and Jae-Ho Chung*
Department of Physics, Korea University, Seoul 136-713, South Korea

Hyun Wook Kang, Su Jae Kim, and Seongsu Lee
Neutron Science Division, Korea Atomic Energy Research Institute, Daejeon 305-353, South Korea
(Received 27 November 2014; revised manuscript received 24 December 2014; published 3 February 2015)

We report large orthorhombic distortions in the ferrimagnetic tetragonal ($c > a$) spinel $Cu_xMn_{3-x}O_4$ stabilized by a few percent of Cu doping. The orthorhombic strains of the ferrimagnetic phases increased linearly to the doping and reached up to $\epsilon \approx 8.2 \times 10^{-3}$ for $x = 0.19$, which is three times larger than the saturated value under external magnetic fields. For high doping ($x \gtrsim 0.17$), the distortions first appeared in the paramagnetic phases and underwent further enhancement simultaneously with the onset of the noncollinear ferrimagnetic ordering. We present the rich magnetostructural phase diagram of $Cu_xMn_{3-x}O_4$, and argue that the diluted t_2 orbital degeneracy of Cu^{2+} under tetrahedral crystal field breaks the global symmetry and triggers the orthorhombic instability inherent in Mn_3O_4.

DOI: 10.1103/PhysRevB.91.064404 PACS number(s): 75.25.Dk, 61.05.F−

I. INTRODUCTION

In transition-metal oxides, strong quantum correlations among interacting electrons play important roles in establishing ground states. Examples of unconventional phenomena revealing such states include metal-insulator transitions [1], orbital ordering [2,3], spin-Peierls-like effects [4,5], or magnetoelectric multiferroics [6,7]. Antiferromagnetic (AFM) exchange interactions are particularly relevant to complex couplings between electronic degrees of freedom because it is not always possible to satisfy all of them imposed on crystal lattices [8]. Structural lattice distortions often provide pathways to overcome these magnetic frustrations and achieve new coupled ground states.

Spinel oxides (AB_2O_4) represent some of the best known systems for observing couplings of spin degrees of freedom to orbitals and/or lattices [9–18]. Crystallographically, their A sites form diamond lattices while B sites form corner-shared networks of tetrahedra or pyrochlore lattices as shown in Fig. 1(a). In the latter, each tetrahedron is made of six nearest-neighbor B-B bonds that are oriented along diagonal directions of the cubic faces. Under cubic symmetry, AFM exchanges between these bonds cannot simultaneously be satisfied and the system becomes fully frustrated with global degeneracy [19]. The natural route to overcome the degeneracy may be contractions along one of the primary axes, or $c < a = b$, upon which four out of six AFM bonds may be satisfied. The relevant spin-lattice couplings are observed in ACr_2O_4 (A = Zn, Mg) with no orbital degrees of freedom involved [5,12]. In contrast, symmetry-lowering distortions may end up satisfying only two AFM bonds when orbital degrees of freedom are involved. Good examples are found in AV_2O_4 (A = Zn, Mg, Mn) with V^{3+} ($3d^2$), in which tetragonal contractions are caused by e_g electrons selectively occupying xy orbitals [14–16]. Similar situations arise also in AMn_2O_4 (A = Zn, Mn) with Mn^{3+} ($3d^4$), in which tetragonal elongations ($c > a = b$) occur due to Jahn-Teller ordering of t_{2g} electrons [20]. Commonly in these cases the exchange overlaps will be relatively weaker along c axes [21], and thus AFM exchanges may be satisfied within c planes. When AFM chains form accordingly, however, the exchanges along the c axes will effectively become canceled. This thus suggests that geometrical frustrations may not be fully removed under such lattice symmetry, and further symmetry-lowering distortions may follow.

Recently, weak orthorhombic lattice distortions were reported below T_N of ferrimagnetic (FIM) Mn_3O_4, in which large tetragonal elongation existed ($c/a = 1.16$) due to the t_{2g} Jahn-Teller ordering [22–24]. In single crystals, the distortion occurred along the [1 0 0] direction, or $a > b$ in the face-centered cell, at around 20 K in zero magnetic field, and the size of the associated strain was $\epsilon = (a - b)/(a + b) = 5 \times 10^{-4}$ [22,23]. When external magnetic field was applied, the strain was enlarged by up to fivefold and the onset temperature was enhanced [23,25,26]. In polycrystals, a high-resolution synchrotron x-ray diffraction revealed partial orthorhombic distortions below T_N [24]. These results consistently indicate that the orthorhombic lattice instability is inherent in Mn_3O_4. The magnetic ground state of Mn_3O_4 is noncollinear Yafet-Kittel (YK) ordering involving one Mn^{2+}(A) and two Mn^{3+}(B) spins [see Fig. 1(b)] [27]. When the spin components parallel to the net magnetization are subtracted, this leaves AFM chains on the B sites. Therefore, geometrical frustrations must still be present in their ordering. Additional orthorhombic distortions can lift the associated degeneracy and must thus be compatible with removal of the frustration.

An obvious way to break the tetragonal symmetry is to apply external magnetic fields, which has already been well studied in Mn_3O_4 [23,25,26,28]. In this work, we investigated a different route to extrinsically break the tetragonal symmetry. We introduced the orbital degeneracy via doping of transition metal ions with different electron configurations. In stoichiometric Mn_3O_4 with strong Hund's coupling, tetrahedral Mn^{2+} ($e^2t_2^3$) and octahedral Mn^{3+} ($t_{2g}^3e_g^1$) ions possess no orbital degeneracies at low temperatures. Under the tetrahedral crystal field, the $3d$ orbitals split into lower e and higher t_2 levels. When the lattice is elongated along the c axis, the t_2 levels will again split into lower (xy) and higher doubly degenerate

*jaehc@korea.ac.kr

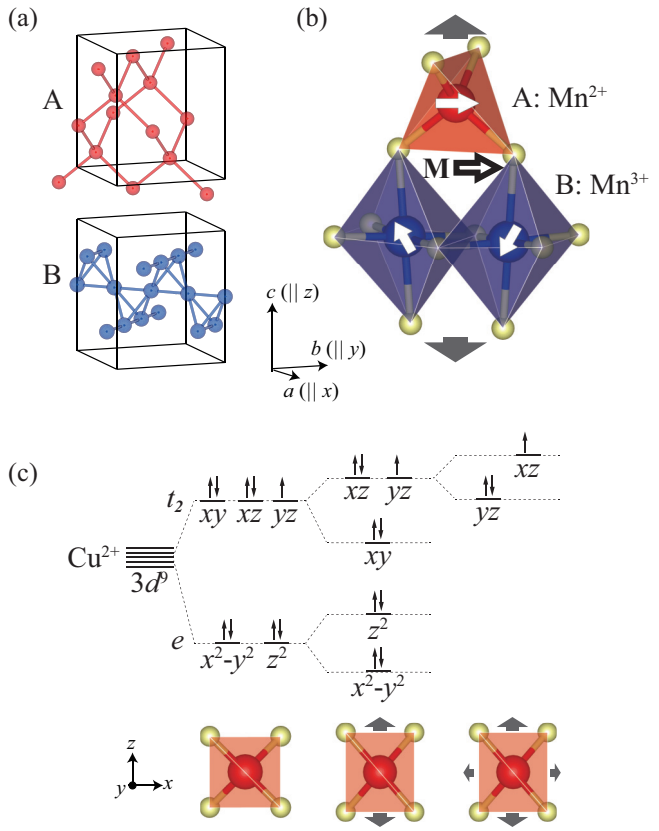

FIG. 1. (Color online) (a) The substructures formed by A and B sites of the spinel lattice. The boxes represent the face-centered $Fddd$ (or $Fd\bar{3}m$ for cubic) unit cell. (b) A portion of the spinel lattice displaying tetrahedral (A) and octahedral (B) sites. Thick gray arrows mark the direction of Jahn-Teller distortion in Mn_3O_4, and white arrows show spins in its YK ordering. (c) Electronic configurations of Cu^{2+} ($3d^9$) in the tetrahedral crystal fields under cubic, tetragonal ($c > a = b$), and orthorhombic ($c > a > b$) symmetries, respectively. Thick gray arrows indicate directions of corresponding lattice distortions.

(xz and yz) levels [see Fig. 1(c)] [29]. This thus provides opportunities to break the fourfold symmetry by partially filling the doubly degenerate levels. The suitable candidate is Cu^{2+} ions with $3d^9$, since they are one electron short of completely filling the $3d$ bands. Based on this idea, in this work we investigated the crystal and magnetic structures of $Cu_xMn_{3-x}O_4$ and $Ni_xMn_{3-x}O_4$ using neutron and x-ray power diffraction methods in the absence of external magnetic field.

II. EXPERIMENTAL

Powder samples of $Cu_xMn_{3-x}O_4$ ($0.0 \leqslant x \leqslant 0.19$) were synthesized by the standard solid state method. The mixtures of high-purity Mn_3O_4 and CuO powders were thoroughly ground and heated to 1050 K. After overnight annealing, the samples were quenched in air. In addition, $Ni_xMn_{3-x}O_4$ samples were also synthesized by mixing Mn_3O_4 and NiO for the purpose of comparison. The dc magnetization measurements were performed using the vibrating sample magnetometry option of Quantum Design's Physical Property Measurement System.

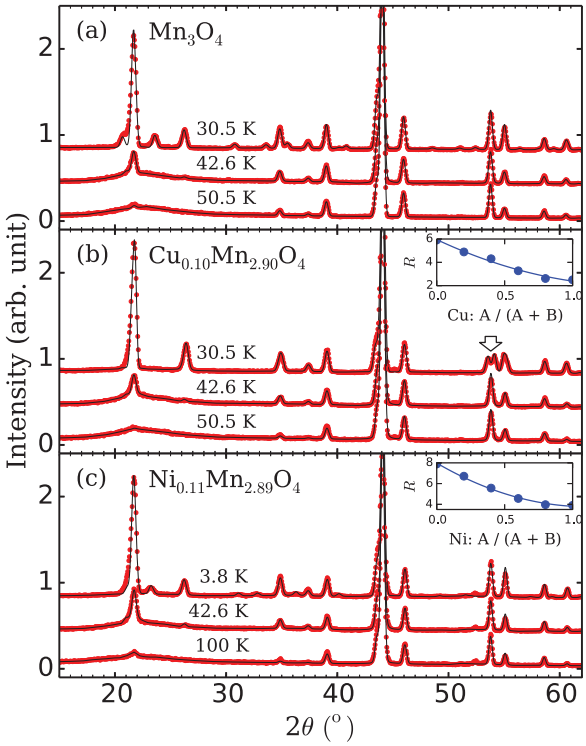

FIG. 2. (Color online) Neutron diffraction intensities of (a) Mn_3O_4, (b) $Cu_{0.10}Mn_{2.90}O_4$, and (c) $Ni_{0.11}Mn_{2.89}O_4$ at selected temperatures representing paramagnetic ($T \geqslant 50.5$ K), Néel ($T = 42.6$ K), and YK ($T \leqslant 30.5$ K) phases. Solid lines through data are best-fit curves by the Rietveld refinement. Insets show the residual factors as a function of dopant fraction on the A sites. In (b), the vertical arrow points to splitting of the (4 0 0)/(0 4 0) doublet.

Neutron powder diffraction measurements were performed using the High-Resolution Powder Diffractometer of the Korea Atomic Energy Research Institute. The samples were filled in thin vanadium tubes using He gas for thermal exchange, and the temperature was controlled using a He closed-cycle refrigerator down to 4 K. Monochromatic neutron beams of the wavelength $\lambda = 1.8345$ Å were produced using the Ge(331) monochromator, and the scattered neutrons were collected by using 32 He^3 proportional counters. The Rietveld refinement was performed using the FULLPROF suite [30]. X-ray powder diffraction measurements were performed using a PANalytical Empyrean diffractometer with Cu Kα radiation ($\lambda = 1.5406$ Å). The Bragg-Brentano geometry was used, in which the sample temperature was controlled down to 15 K by a He closed-cycle refrigerator.

III. RESULTS

Plotted in Fig. 2 are the neutron diffraction intensities at selected temperatures representing distinctive magnetic phases of Mn_3O_4, $Cu_{0.10}Mn_{2.90}O_4$, and $Ni_{0.11}Mn_{2.89}O_4$. For all samples above 50 K, the neutron diffraction intensities could be reasonably fitted by using the structural model based on the tetragonal $I4_1amd$ unit cell. Magnetic intensities in this temperature range were observed only as broad diffuse peaks at low angles. At $T = 42.6$ K, Bragg peaks at low angles exhibited noticeable intensity increases indicating the

appearance of collinear Néel FIM ordering [27]. In this ordering, magnetic moments of the A and B sites are oriented antiparallel to each other.

Upon further cooling, striking differences emerge between the undoped and Cu-doped samples. At $T = 30.5$ K, several magnetic Bragg peaks showed up for Mn_3O_4. The peak at $2\theta = 26.3^\circ$ corresponds to $Q = (0\ 2\ 0)$, which indicates that the spins on the B sites deviated from being collinear and developed AFM chain components. Combined with the Néel ordering, they compose the YK ordering as shown in Fig. 1(b). Additional peaks at $2\theta = 23.6^\circ$ or 30.8° account for the cell-doubling (CD) modulation of the AFM chains, which is the well-known characteristic feature of undoped Mn_3O_4 [27]. In contrast, $Cu_{0.10}Mn_{2.90}O_4$ did not show the CD peaks but exhibited splitting of structural Bragg peaks at high angles. The doublet observed at $2\theta = 54^\circ$ corresponds to (4 0 0) and (0 4 0) reflections, respectively, and thus indicates that the tetragonal symmetry of the Mn_3O_4 lattice has indeed been fully broken. In Fig. 2(b), the solid line through the neutron diffraction data at $T = 30.5$ K was the best-fit curve by using the orthorhombic $Fddd$ unit cell.

Copper ions can occupy either tetrahedral or octahedral sites in spinel lattices, which is well known from large site mixing of cubic $CuMn_2O_4$ [31]. Based on the residual factors from the Rietveld refinements, however, we conclude that they primarily occupied the A sites over the doping range investigated (see insets in Fig. 2). It is also important to emphasize that $Ni_{0.11}Mn_{2.89}O_4$ did not undergo orthorhombic distortions but showed qualitatively similar behaviors with respect to Mn_3O_4 [see Fig. 2(c)]. Note that the Cu^{2+} and Ni^{2+} ions under the tetrahedral crystal field are supposed to have t_2^5 and t_2^4 electrons, respectively. When the lattice is elongated along the c axis, the highest t_2 doublets of Cu^{2+} should accommodate an odd number of electrons whereas those of Ni^{2+} an even number [see Fig. 1(c)]. As a result, orbital degeneracy introduced by Cu^{2+} will break the fourfold symmetry and cause the symmetry-lowering distortion, which is not available by Ni^{2+}. The apparent absence of orthorhombic distortion in $Ni_{0.11}Mn_{2.89}O_4$ supports the picture of doped orbital degeneracy.

We remind the reader that weak orthorhombicity was previously reported in undoped Mn_3O_4 as well [22,24]. The present neutron diffraction data consistently suggested such distortions although the resolution was not sufficient. In order to visualize how the distortions enhance with doping, we show the representative data in Fig. 3 illustrating magnetic and structural phase transitions of $Cu_xMn_{3-x}O_4$. In Mn_3O_4, three successive changes were observed in the dc magnetization, $M(T)$, representing Néel ($T_N = 42.5$ K) and two YK ordering transitions with incommensurate ($T_1 = 39.5$ K) and commensurate ($T_2 = 34.4$ K) CD modulations, respectively [see Fig. 3(a)] [27]. They were visible more clearly in the temperature derivative of the magnetization, dM/dT, shown in Fig. 3(b). As Cu doping was introduced, the YK ordering transitions changed noticeably although T_N was hardly affected. For $x = 0.025$, T_1 shifted down to 38 K but the CD ordering remained incommensurate down to 4 K. Instead, a new dip associated with the orthorhombic distortion was observed in dM/dT at $T = 34$ K suggesting establishment of new magnetic ordering. The orthorhombic phase coexisted

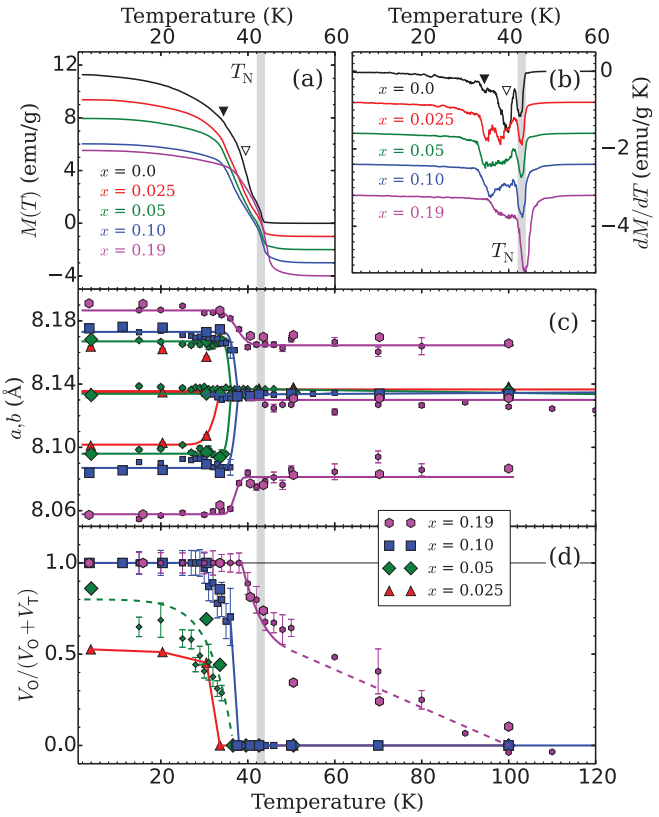

FIG. 3. (Color online) Temperature dependencies of (a) dc magnetization and (b) its temperature derivative, (c) lattice parameters, and (d) orthorhombic volume fractions for $Cu_xMn_{3-x}O_4$. The $M(T)$ curves in (a) and (b) were measured in zero field following cooling under $B = 100$ G. The gray areas show T_N, while the closed and open triangles mark YK ordering transitions of Mn_3O_4 with incommensurate (T_1) and commensurate (T_2) CD modulations, respectively. In (c) and (d), data shown with larger symbols were obtained by the Rietveld refinement of neutron diffraction intensities and are thus considered to have high accuracy. The data shown with smaller symbols were obtained by converting scattering angles and integrated intensities of (4 0 0)/(0 4 0) peaks from x-ray diffraction data. In (c), these values were scaled to the neutron data. The solid and dashed lines are guides to the eye.

with the tetragonal, and its volume fraction remained nearly constant at ~0.5 below 30 K [see Fig. 3(d)]. This volume fraction is similar to the value of undoped Mn_3O_4 reported by the synchrotron x-ray diffraction [24]. It was enhanced to ~0.85 for $x = 0.05$ and finally became unity for $x = 0.10$. The disappearance of the tetragonal phase for $x = 0.10$ at low temperatures is clearly seen in the x-ray and neutron diffraction intensities, which are plotted in Figs. 4(a) and 4(c). The magnitude of orthorhombic distortion continued to increase with doping, while the the onset temperature was only marginally enhanced. For all samples with $x \leqslant 0.10$, the orthorhombic phases appeared at temperatures well below T_N but only slightly below the YK ordering transitions. Such correspondence reflects close relations between the stabilization of the AFM chains and the observed orthorhombic distortions.

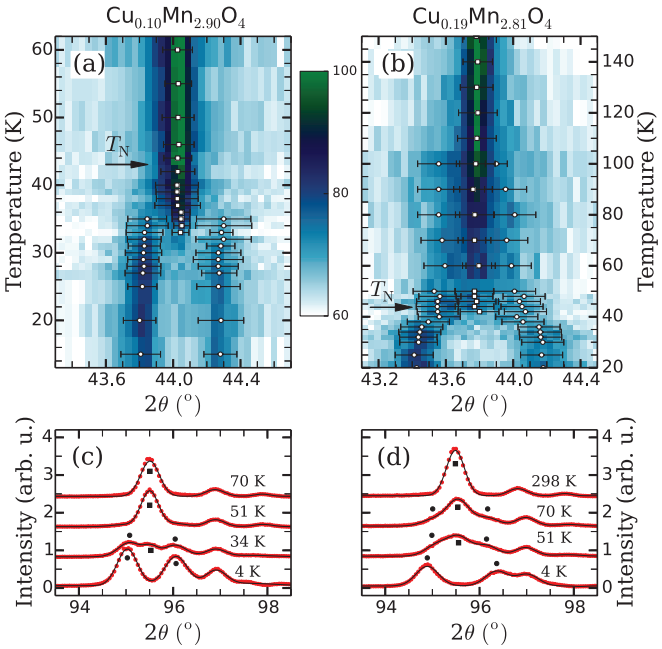

FIG. 4. (Color online) The upper panels show the temperature-dependent x-ray powder diffraction intensities of (4 0 0)/(0 4 0) Bragg peaks for (a) $Cu_{0.10}Mn_{2.90}O_4$ and (b) $Cu_{0.19}Mn_{2.81}O_4$. The empty squares and circles mark the fitted peak positions, and the error bars show their full widths at half maxima. The lower panels show the neutron powder diffraction intensities of (6 2 2)/(2 6 2) Bragg peaks for (c) $Cu_{0.10}Mn_{2.90}O_4$ and (d) $Cu_{0.19}Mn_{2.81}O_4$.

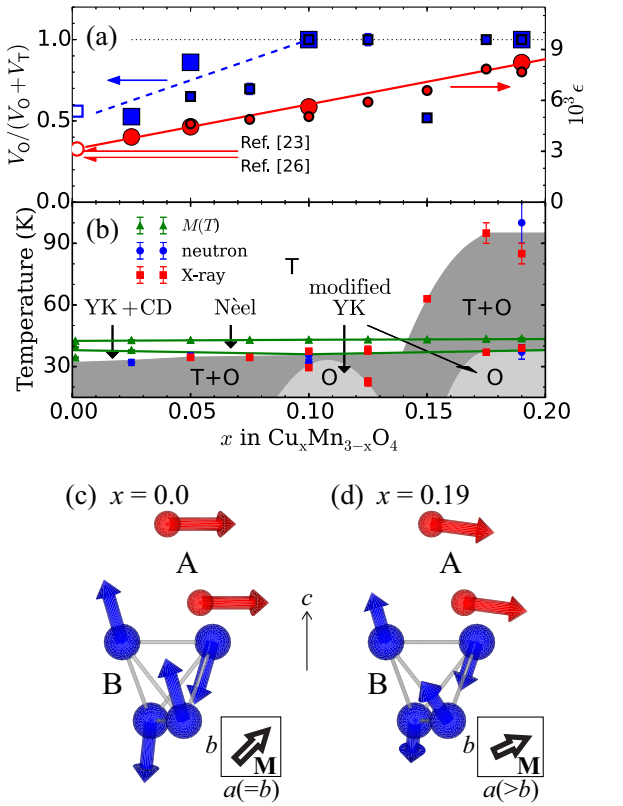

FIG. 5. (Color online) (a) Doping dependencies of the orthorhombic volume fractions and lattice strains of $Cu_xMn_{3-x}O_4$. Large and small filled symbols represent data from neutron (4 K) and x-ray diffraction (15 K), respectively. Empty symbols of the same kinds are the synchrotron x-ray data from Ref. [24]. The two long half arrows mark the high-field strains in single crystals from Refs. [23] and [26], respectively. The solid line through the strains is the linear fit, whereas the dashed and dotted lines are guides to the eye. (b) The magnetostructural phase diagram of $Cu_xMn_{3-x}O_x$. T and O are short for tetragonal and orthorhombic phases, respectively. Shown in (c) and (d) are magnetic structures at 4 K for $x = 0.0$ (tetragonal) and $x = 0.19$ (orthorhombic), respectively. The structure shown in (d) represents the modified YF of the phase diagram in (b). The respective net magnetization vectors are shown at right bottom corners.

We observed, however, that the orthorhombic distortion was not strictly limited to below T_N for higher doping. For $x = 0.19$, the peaks corresponding to the orthorhombic structure first appeared near 90 K and coexisted with the tetragonal phase [see Figs. 4(b) and 4(d)]. During cooling its volume fraction gradually increased but the orthorhombic strain remained constant. As the YK ordering was setting in near 40 K, whole volume became orthorhombic and the distortion was further enhanced [also see Figs. 3(c) and 3(d)]. These two-step transitions show that the orbital degeneracy of Cu^{2+} ions first couples to the lattice and subsequently interact with the spin degree of freedom. Such behavior is a clear signature of cooperative spin-orbital-lattice couplings mediated by the doped t_2 degeneracy. At low temperatures, the orthorhombic strain became as large as $\epsilon = 8.2 \times 10^{-3}$ for $x = 0.19$, which is nearly three times larger than the saturated strain under external magnetic fields ($B \geqslant 1$ T) [23,26]. As shown in Fig. 5(a), it is notable that the orthorhombic strain exhibited linear dependence on x for the whole doping range investigated.

IV. DISCUSSION

In fact, the orthorhombic lattice symmetries are already known for certain spinel oxides, and many of them contain Cu^{2+} on their A sites [32–39]. One of the representative cases with tetrahedral Cu^{2+} is FIM $CuCr_2O_4$, whose lattice above T_N is tetragonal. Recently, a magnetostructural orthorhombic distortion was observed by synchrotron x-ray diffraction [35]. The magnitude of the associated lattice strains, however, was reported to be smaller than 10^{-3}. In other works, similar distortions were also reported in AFM ACr_2O_4 (A = Mg, Zn) doped with Cu^{2+} [36,37]. In these chromates, tetragonal distortions originally occur at T_N by c-axis contractions. Since the tetrahedral higher t_2 level is not doubly degenerate in this case, the observed orthorhombic strains were barely 10^{-3} at best [36,37]. The present result is directly comparable to the large orthorhombic strain ($>10^{-2}$) observed in $Cu_xNi_{1-x}Cr_2O_4$ for $x = 0.15$ or higher [38,39]. In this system, the orthorhombic phase was stable only over a very narrow range of composition because Cr^{3+} ($3d^3$) ions in the B sites contributed to no orbital degeneracy [38]. This is in contrast to $Cu_xMn_{3-x}O_4$ of the present work, for which Mn^{3+} ions provides stable Jahn-Teller ordering over a wide range of composition.

Suzuki *et al.* have previously explained the field-induced distortion in terms of the spin-orbital coupling of the octahedral Mn^{3+} ions [25]. In this scenario, lattice elongation occurs when the rotation of net magnetization under $B \parallel a$ causes partial

transfer of e_g electrons from z^2 to x^2 orbital. In contrast, the current results represent the case in which orbital degeneracy of doped Cu^{2+} ions spontaneously couples to the lattice and/or spin and breaks the global fourfold symmetry. We have previously proposed the geometrical frustrations of stacked AFM chains to be responsible for the structural instability [22]. The giant orthorhombic distortions revealed in this work corroborate the picture of the preexisting lattice instability in Mn_3O_4. It remains yet to be seen whether or not the true t_2 orbital ordering of doped Cu^{2+} ions was established. The plot in Fig. 5(a) also insinuates that the zero-field strains observed in the present work are closely related to the field-induced strain of the pristine Mn_3O_4. Interestingly, when the present data were linearly extrapolated down to $x = 0$, they closely coincided with both the zero-field [24] and high-field [23,26] strains of Mn_3O_4 [see Fig. 5(a)]. The field effect was to stabilize the orthorhombic symmetry but not to enhance the strain. This thus strongly suggests the possibility that the field-induced orthorhombic distortion could have occurred by symmetry breaking without necessity of orbital hybridization [25].

Finally, we summarize the results in the form of the magnetostructural phase diagram shown in Fig. 5(b). It shows that the orthorhombic phases become fully stable at two separated regions, one near $x \sim 0.11$ and the other $x \gtrsim 0.17$. Such behavior is visible also from the volume fraction of $x = 0.15$ less than unity shown in Fig. 5(a). It is around this region where the paramagnetic phase begins to show orthorhombic distortions. This is a signature of the reentrant phase instability upon reorganizing competitions among orbital, lattice, and spin degrees of freedom. Also depicted in Fig. 5(c) are the magnetic structures of the tetragonal and orthorhombic phases obtained by the Rietveld refinement. Given that $a > b$, the presence (or absence) of the (0 2 0) [or (2 0 0)] Bragg peaks in neutron diffraction data confirms that the chains are stacked by satisfying AFM correlations along the shorter bonds. The best-fit results, however, did not indicate the presence of such simple magnetic structures. Given the constraint that the net moments of A and B sites are oriented opposite to each other, the alignment of the AFM components between the longer bonds were not exactly parallel to but tilted away from each other [see Fig. 5(d) and Table I]. Such nontrivial magnetic ordering suggests that the nearest-neighbor interactions are not sufficient for understanding the complex magnetism of Mn_3O_4.

TABLE I. Summary of crystallographic and magnetic structural parameters at 4 K obtained by the Rietveld refinement of the neutron powder diffraction data. The polar angle θ is the inclination off the c axis, and the azimuthal angle ϕ is the counterclockwise rotation from the a axis of the $Fddd$ unit cell. The fractional coordinates of the listed ions are given as follows. A1: (1/8, 1/8, 1/8), A2: (7/8, 7/8, 7/8), B1: (1/2, 1/2, 1/2), B2: (1/4, 1/4, 1/2), B3: (1/4, 1/2, 1/4), B4: (1/2, 1/4, 1/4).

	$x =$	0.0	0.10	0.19
a		8.1370(1)	8.1752(1)	8.1910(2)
b		8.1370(1)	8.0839(1)	8.0573(2)
c		9.4351(2)	9.4165(1)	9.4097(2)
A1/A2	m (μ_B)	4.41(7)	4.44(5)	3.83(10)
	θ (°)	90	84(8)	93(7)
	ϕ (°)	45	22(4)	19(6)
B1	m (μ_B)	3.67(5)	3.24(16)	3.09(10)
	θ (°)	154(5)	156(15)	118(2)
	ϕ (°)	225	203(8)	192(8)
B2	m (μ_B)	3.67(5)	3.00(11)	3.29(7)
	θ (°)	26(5)	28(11)	62(2)
	ϕ (°)	225	202(8)	207(9)
B3	m (μ_B)	2.29(5)	2.72(12)	3.49(10)
	θ (°)	27(9)	29(13)	69(2)
	ϕ (°)	225	257(11)	244(9)
B4	m (μ_B)	2.29(5)	3.48(11)	2.86(11)
	θ (°)	153(9)	140(7)	113(2)
	ϕ (°)	225	174(7)	122(7)

V. CONCLUSIONS

In conclusion, large orthorhombic distortions ($\epsilon \gg 10^{-3}$) were observed in FIM spinel Mn_3O_4 doped with Cu^{2+} on 20% or less of its tetrahedral sites. The associated strains showed a linear dependence on the doping concentration and consistently exhibited major increases upon onsets of the noncollinear ferrimagnetic ordering. Given the twofold degeneracy in the higher t_2 levels under elongated tetragonal symmetry, the Cu^{2+} $3d^9$ ions provide an odd number of electrons to these levels and cause the orthorhombic distortion. This is in contrast to Ni^{2+} $3d^8$ with even number, for which no orthorhombic distortions were detected in our measurements. Our current work presents an interesting example in which externally introduced dilute orbital degeneracy couples to the intrinsic spin and/or lattice degrees of freedom and governs the global structural symmetry.

ACKNOWLEDGMENTS

This work was financially supported by the National Research Foundation of Korea (NRF) grants funded by the Korea Government (MSIP) through the ARCNEX (NRF-2011-0031933) and the Nuclear R&D Programs (NRF-2013M2A2A6029081 and 2012M2A2A6002461).

[1] M. Imada, A. Fujimori, and Y. Tokura, Rev. Mod. Phys. **70**, 1039 (1998).
[2] T. Hotta, Rep. Prog. Phys. **69**, 2061 (2006).
[3] K. Gupta, P. Mahadevan, P. Mavropoulos, and M. Ležaić, Phys. Rev. Lett. **111**, 077601 (2013).
[4] G. Castilla, S. Chakravarty, and V. J. Emery, Phys. Rev. Lett. **75**, 1823 (1995).
[5] S.-H. Lee, H. Takagi, D. Louca, M. Matsuda, S. Ji, H. Ueda, Y. Ueda, T. Katsufuji, J.-H. Chung, S. Park, S.-W. Cheong, and C. Broholm, J. Phys. Soc. Jpn. **79**, 011004 (2010).
[6] S. Lee, A. Pirogov, M. Kang, K.-H. Jang, M. Yonemura, T. Kamiyama, S.-W. Cheong, F. Gozzo, N. Shin, H. Kimura, Y. Noda, and J.-G. Park, Nature (London) **451**, 805 (2007).

[7] X. Fabrèges, S. Petit, I. Mirebeau, S. Pailhès, L. Pinsard, A. Forget, M. T. Fernandez-Diaz, and F. Porcher, Phys. Rev. Lett. **103**, 067204 (2009).
[8] J. T. Chalker, in *Introduction to Frustrated Magnetism*, edited by C. Lacroix, P. Mendels, and F. Mila (Springer-Verlag, Berlin, 2011), Chap. 1.
[9] S. Ji, S.-H. Lee, C. Broholm, T. Y. Koo, W. Ratcliff, S.-W. Cheong, and P. Zschack, Phys. Rev. Lett. **103**, 037201 (2009).
[10] J.-H. Chung, M. Matsuda, S.-H. Lee, K. Kakurai, H. Ueda, T. J. Sato, H. Takagi, K.-P. Hong, and S. Park, Phys. Rev. Lett. **95**, 247204 (2005).
[11] H. Ueda, H. Mitamura, T. Goto, and Y. Ueda, Phys. Rev. B **73**, 094415 (2006).
[12] L. Ortega-San-Martín, A. J. Williams, C. D. Gordon, S. Klemme, and J. P. Attfield, J. Phys.: Condens. Matter **20**, 104238 (2008).
[13] M. Schmidt, W. Ratcliff, P. G. Radaelli, K. Refson, N. M. Harrison, and S.-W. Cheong, Phys. Rev. Lett. **92**, 056402 (2004).
[14] S.-H. Lee, D. Louca, H. Ueda, S. Park, T. J. Sato, M. Isobe, Y. Ueda, S. Rosenkranz, P. Zschack, J. Íñiguez, Y. Qiu, and R. Osborn, Phys. Rev. Lett. **93**, 156407 (2004).
[15] E. M. Wheeler, B. Lake, A. T. M. N. Islam, M. Reehuis, P. Steffens, T. Guidi, and A. H. Hill, Phys. Rev. B **82**, 140406(R) (2010).
[16] T. Suzuki, M. Katsumura, K. Taniguchi, T. Arima, and T. Katsufuji, Phys. Rev. Lett. **98**, 127203 (2007).
[17] T. Katsufuji, T. Suzuki, H. Takei, M. Shingu, K. Kato, K. Osaka, M. Takata, H. Sagayama, and T.-H. Arima, J. Phys. Soc. Jpn. **77**, 053708 (2008).
[18] P. T. Barton, M. C. Kemei, M. W. Gaultois, S. L. Moffitt, L. E. Darago, R. Seshadri, M. R. Suchomel, and B. C. Melot, Phys. Rev. B **90**, 064105 (2014).
[19] H. Takagi and S. Nitaka, in *Introduction to Frustrated Magnetism*, edited by C. Lacroix, P. Mendels, and F. Mila (Springer-Verlag, Berlin, 2011), Chap. 7.
[20] J. B. Goodenough and A. L. Loeb, Phys. Rev. **98**, 391 (1955).
[21] J.-H. Chung, J.-H. Kim, S.-H. Lee, T. J. Sato, T. Suzuki, M. Katsumura, and T. Katsufuji, Phys. Rev. B **77**, 054412 (2008).
[22] J.-H. Chung, K. H. Lee, Y.-S. Song, T. Suzuki, and T. Katsufuji, J. Phys. Soc. Jpn. **82**, 034707 (2013).
[23] J.-H. Chung, H. Chang, H. B. Lee, K. H. Lee, K. Prokes, S. Mat'as, T. Suzuki, and T. Katsufuji (unpublished).
[24] M. C. Kemei, J. K. Harada, R. Seshadri, and M. R. Suchomel, Phys. Rev. B **90**, 064418 (2014).
[25] T. Suzuki and T. Katsufuji, Phys. Rev. B **77**, 220402(R) (2008).
[26] Y. Nii, H. Sagayama, H. Umetsu, N. Abe, K. Taniguchi, and T. Arima, Phys. Rev. B **87**, 195115 (2013).
[27] G. B. Jensen and O. V. Nielsen, J. Phys. C: Solid State Phys. **7**, 409 (1974).
[28] M. Kim, X. M. Chen, X. Wang, C. S. Nelson, R. Budakian, P. Abbamonte, and S. L. Cooper, Phys Rev. B **84**, 174424 (2011).
[29] I. B. Goldberg and T. M. McKinney, in *Laboratory Techniques in Electroanalytical Chemistry*, edited by P. Kissinger and W. Heineman (Marcel Dekker, New York, 1996), Chap. 29.
[30] J. Rodríguez-Carvajal, Physica B **192**, 55 (1993).
[31] A. Waśkowska, L. Gerward, J. Staun Olsen, S. Steenstrup, and E. Talik, J. Phys.: Condens. Matter **13**, 2549 (2001).
[32] M. H. Francomne, J. Phys. Chem. Solids **3**, 37 (1957).
[33] V. N. Glazkov, A. M. Farutin, V. Tsurkan, H.-A. Krug von Nidda, and A. Loidl, Phys. Rev. B **79**, 024431 (2009).
[34] M. C. Kemei, P. T. Barton, S. L. Moffitt, M. W. Gaultois, J. A. Kurzman, R. Seshadri, M. R. Suchomel, and Y.-I. Kim, J. Phys.: Condens. Matter **25**, 326001 (2013).
[35] M. R. Suchomel, D. P. Shoemaker, L. Ribaud, M. C. Kemei, and R. Seshadri, Phys. Rev. B **86**, 054406 (2012).
[36] D. P. Shoemaker and R. Seshadri, Phys. Rev. B **82**, 214107 (2010).
[37] M. C. Kemei, S. L. Moffitt, L. E. Darago, R. Seshadri, M. R. Suchomel, D. P. Shoemaker, K. Page, and J. Siewenie, Phys. Rev. B **89**, 174410 (2014).
[38] A. Wold, R. J. Arnott, E. Whipple, and J. B. Goodenough, J. Appl. Phys. **34**, 1085 (1963).
[39] M. Tovar, R. Torabi, C. Welker, and F. Fleischer, Physica B: Condens. Matter **385-386**, 196 (2006).